Static and dynamic spectroscopy of (Al,Ga)As/GaAs microdisk lasers with interface fluctuation quantum dots

W. H. Wang,[1] S. Ghosh,[2] F. M. Mendoza,[2] X. Li,[1] D. D. Awschalom,[2] and N. Samarth[1,2,*]
[1]*Materials Research Institute, Penn State University, University Park, Pennsylvania 16802, USA*
[2]*Center for Spintronics and Quantum Computation, University of California, Santa Barbara, California 93106, USA*
(Received 12 May 2004; revised manuscript received 2 December 2004; published 7 April 2005)

We have studied the steady state and dynamic optical properties of semiconductor microdisk lasers whose active region contains interface fluctuation quantum dots in GaAs/(Ga,Al)As quantum wells. Steady-state measurements of the stimulated emission via whispering gallery modes yield a quality factor $Q \sim 5600$ and a coupling constant $\beta \sim 0.09$. The broad gain spectrum produces mode hopping between spectrally adjacent whispering gallery modes as a function of temperature and excitation power. Time- and energy-resolved photoluminescence measurements show that the emission rise and decay rates increase significantly with excitation power. Marked differences are observed between the radiative decay rates in processed and unprocessed samples.

DOI: 10.1103/PhysRevB.71.155306 PACS number(s): 78.47.+p, 78.67.Hc, 03.67.Lx, 42.55.Sa

Current interest in quantum information processing has motivated several fundamental studies of the coupling between zero-dimensional (0D) electronic states and confined photon modes in semiconductor microdisks.[1–7] These experiments have focused on high finesse microdisks where the 0D states of self-assembled InAs quantum dots (QDs) couple with the whispering gallery modes (WGMs) of a cylindrical microcavity, and are characterized by a large coupling constant ($\beta \sim 0.1$) between the spontaneous emission and the cavity modes. Because the QD emission is characterized by a narrow homogeneous linewidth while the gain spectrum is characterized by a much larger inhomogeneous broadening,[8] such microdisks exhibit simultaneous stimulated emission from several whispering gallery cavity modes.[6] This behavior contrasts with microdisks containing two-dimensional (2D) quantum-well (QW) states that typically show stimulated emission from a single cavity mode due to the narrower gain width, but suffer from lower Q (typically between $\sim$3000 and $\sim$5000) because of larger absorption in the QW.[9,10] Here, we discuss the spontaneous and stimulated emission from microdisks that lie in an intermediate regime, where the active region contains interface fluctuation quantum dots (IFQDs) within narrow GaAs quantum wells.[11–13] This design drastically reduces the number of modes that lase simultaneously, while allowing for a relatively high Q factor ($Q \sim 5600$) and large coupling constant ($\beta \sim 0.09$). We note that although recent experiments have studied triggered single-photon emission from IFQDs incorporated into patterned disks, we are unaware of any demonstrated mode coupling and/or stimulated emission in such structures.[14]

The microdisks in this study are patterned from GaAs/(Ga,Al)As heterostructures grown by molecular beam epitaxy (MBE) on (001) semi-insulating GaAs substrates. The samples consist of a 120-nm-thick GaAs buffer layer, a 500-nm-thick $Al_{0.8}Ga_{0.2}As$ pedestal layer, and finally a 110-nm-thick $Al_{0.31}Ga_{0.69}As$/GaAs heterostructure that forms the microdisk itself. The microdisk region contains an optically active region with six 4.2-nm-thick GaAs QWs, isolated from each other by 10-nm-thick $Al_{0.31}Ga_{0.69}As$ barriers. This optically active region is sandwiched between 38-nm-thick $Al_{0.31}Ga_{0.69}As$ layers. At each interface, growth interruptions of 30 s are used to induce IFQDs. As shown in Fig. 1(a) (top), low-temperature microphotoluminescence (micro-PL) measurements on such samples reveal sharp spectral features with a full width at half maximum (FWHM) limited by the resolution of our spectrometer ($\sim$200 μeV).

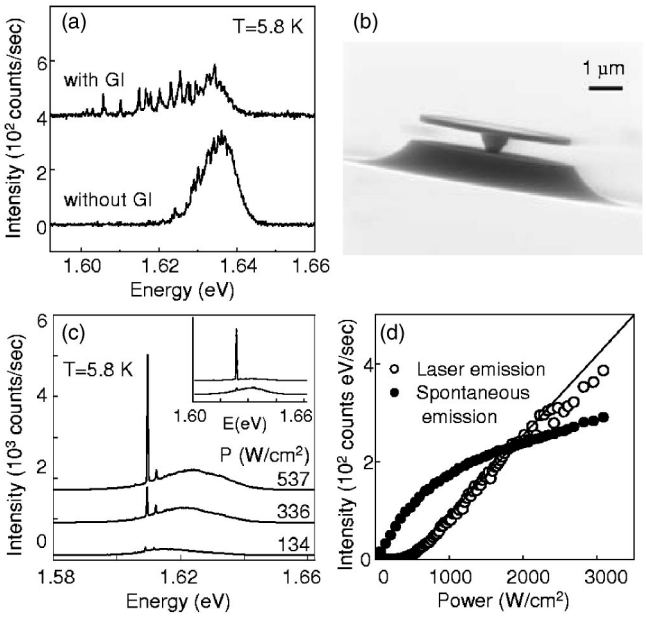

FIG. 1. (a) Microphotoluminescence measurements carried out on unpatterned samples through a 1 μm diameter gold aperture. Resolution-limited spectral features characteristic of QD states (FWHM$\leqslant$200 μeV) are only seen in the sample with growth interruptions. (b) SEM image of microdisk laser structure. (c) Excitation power dependence of the emission spectrum of a single microdisk at $T=5.8$ K. The inset shows the polarization-resolved far field emission from the side of a single microdisk. The top and the bottom spectra are polarization parallel and perpendicular to the disk plane. (d) Intensity of the stimulated emission (mode $TE_{35,1}$) and spontaneous emission vs pump power, respectively.

 ©2005 The American Physical Society

We also fabricated control samples with the optically active region containing either 10-nm-wide QWs or 4.2 nm QWs with no growth interruptions. In the former, the confined electronic states are explicitly 2D and do not show any spectral structure in micro-PL measurements, while in the latter the density and extent of the lateral 0D confining region is highly reduced, and there are only weak signs of spectral structure in the micro-PL [Fig. 1(a) (bottom)].

Microdisks are processed from the MBE-grown wafers using standard photolithography procedures, followed by a two-step HBr and $(NH_4)_2S$ wet chemical etch. In the first step, a nonselective HBr-based mesa etch defines the circular portion of the microdisk. The isotropic etching characteristics of HBr reduce the disk diameter by approximately 1 μm during the etching process. In the second step, the 20–24 % $(NH_4)_2S$ solution with excess sulfur (5 mg/mL) etches the $Al_{0.8}Ga_{0.2}As$ layer with high selectivity, producing microdisks of $\sim$4 μm diameter on narrow pedestals [Fig. 1(b)]. The $(NH_4)_2S$ also passivates the surface states to reduce nonradiative recombination at the microdisk surface. We note that the sole use of $(NH_4)_2S$ for both selective etching and passivation simplifies the overall processing in comparison with past practices that used a separate selective etch, followed by passivation.[9] Further, we use a lower temperature ($\sim$50 °C) for the $(NH_4)_2S$ solution; this appears to improve the passivation of surface states, resulting in a higher radiative efficiency. Finally, we stabilize the sulfide layers by encapsulating the sample with 40 nm SiN_x deposited using electron cyclotron resonance plasma enhanced chemical vapor deposition.

We perform steady-state photoluminescence (PL) measurements using continuous wave (CW) 568 nm excitation from an Ar/Kr mixed gas laser. The samples are mounted on a cold finger in a liquid He continuous flow cryostat, with a temperature sensor comounted on the cold finger close to the sample to monitor heating effects. Both the optical excitation and collection use an objective lens (100×, numerical aperture 0.73) with an excitation spot diameter of 20 μm; the collected PL is spectrally resolved by a monochromator (spectral resolution=180 μeV) and detected by an LN2 cooled charge coupled device detector. Polarization-resolved PL measurements are carried out in the far field in a different optical cryostat. Time-resolved PL measurements are made with similar excitation/collection optics, but the optical pumping is carried out with a pulsed Ti-sapphire laser at 740 nm (repetition rate of 76 MHz and pulse width of 150 fs). The PL is again spectrally resolved with a monochromator, and then temporally resolved using a streak camera, which is phase-locked to the pulsed laser in order to synchronize the sweep pulse of the streak tube with the incoming signal. The time resolution of the streak camera is 2 ps.

Figure 1(c) shows the CW emission spectra of a single microdisk laser for three different excitation powers. At the lowest excitation power, the spectrum is dominated by the spontaneous emission from the active region, but we already see evidence for the coupling of the PL emission to a few cavity modes (identified later as WGMs). As the power increases, one of the WGMs lases, with the onset of lasing defined by a clear threshold [Fig. 1(d)]. The intensity of the integrated PL continues to increase above the lasing threshold; this contrasts with the carrier pinning effect observed in conventional semiconductor lasers and is probably due to the nonequilibrium heating of the gain medium, as has been reported in other high coupling constant microdisks.[15,16] The stimulated emission is observed in the same spectral region where the IFQD features occur in the micro-PL from unprocessed samples. However, we note that—unlike the case of microdisks containing InAs QDs where the QD emission is well-separated from any wetting layer emission—it is difficult to unambiguously identify IFQD states as the sole source of WGM emission.

Because it is not possible to obtain an exact analytical solution for the modes of a cylindrical dielectric slab, we use a well-known approximation that treats the problem as a guided wave with vacuum wavelength λ traveling along the axial direction (z) of a dielectric slab waveguide of refractive index n_{eff}, thickness D, and radius R.[17] The resulting eigenfrequencies are characterized by a set of three mode numbers (m,l,p) corresponding to the azimuthal, radial, and planar degrees of freedom, respectively. We ignore the planar mode number p because only the lowest-order planar mode ($p=0$) in the z direction is allowed by the thin microdisk ($D/\lambda \sim 0.14$). We estimate the refractive index in the axial direction (n_z) from $\tan[k_z D/2]=h/k_z$, where k_z is the wave vector in the z direction, and $k_z^2+h^2 \equiv k^2[n_1^2+n_2^2]$, with n_1 and n_2 being the refractive indices inside and outside the disk structure, respectively. The effective index in the azimuthal direction is then calculated from $n_{\text{eff}}=\alpha\sqrt{n_1^2-n_z^2}$, $\alpha=f-(g/R/\lambda)$ with parameters $f=0.984, g=0.163$ for $l=1$.[17] This results in $n_{\text{eff}} \sim 2.3$, compared to the bulk value $n=3.4$. We then use this value of n_{eff} to estimate the allowed eigenfrequencies by solving the two-dimensional Helmholtz equation, whose solution results in Bessel functions of the first kind.[18] This calculation identifies the laser emission at 1.61 eV as a WGM with TE polarization and $m=35$, $l=1$. The far-field laser emission collected from the side of the microdisk is strongly polarized in the disk plane [inset to Fig. 1(c)], confirming the TE nature of the stimulated emission. We note that selection rules for recombination between conduction-band electrons and heavy holes also produce the same polarization for spontaneous emission in this geometry, suggesting a possible reason for the preferred coupling of the emission to a TE rather than a TM cavity mode.

Figure 2(a) shows a log-log plot of the laser emission intensity in this mode as a function of the excitation intensity I. The laser threshold ($\sim$240 W/cm^2) is indicated by a kink in this plot, highlighted by the arrow. (As a comparison, we note that microdisks patterned from the 4.2 nm and 10 nm QW control samples exhibit somewhat higher thresholds of 410 W/cm^2 and 300 W/cm^2, respectively.) The laser emission intensity is proportional to the photon number p in the mode, which we define as unity at the threshold.[19] To determine the cavity coupling constant β, we fit the data in Fig. 2(a) using the following equation which relates the photon number to the excitation intensity:[20]

$$I(p) = A\left[\frac{p}{1+p}(1+\xi)(1+\beta p) - \xi\beta p\right]. \qquad (1)$$

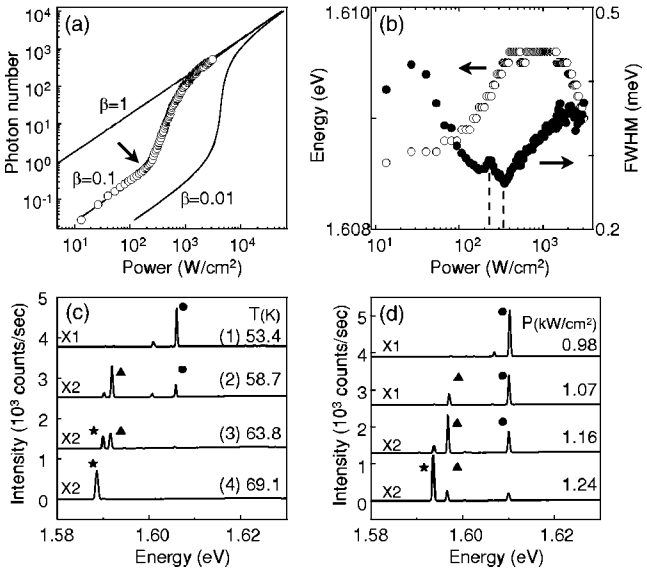

FIG. 2. (a) Power dependence of lasing intensity plotted on a log-log scale. The arrow indicates the laser threshold. Solid curves are based on Eq. (1) with coupling constant $\beta=1,0.1,0.01$. (b) Power dependence of the energy (open circles) and width (solid circles) of the lasing mode. (c) Temperature dependence of microdisk emission spectrum, showing mode hopping between the $TE_{35,1}$ (circle), $TE_{30,2}$ (triangle), and $TE_{26,3}$ (star) WGMs. (d) Pump power dependence of microdisk emission spectra at a sample mount temperature of $T=5$ K.

Here, the scale factor $A=\hbar\omega\gamma/\delta\beta$, where ω is the frequency of the mode, γ is the cavity decay rate, and δ is the photon conversion efficiency. The dimensionless parameter ξ is defined by $\xi=N_0\beta V/\gamma\tau_{sp}$, where N_0 is the transparency carrier concentration of the gain material, V is the volume of the active material, and τ_{sp} is the spontaneous-emission lifetime. The above equation assumes that only one mode lases within the gain region, and that nonradiative recombination is negligible. Since we do not have direct knowledge of several parameters such as γ, N_0, and δ, we treat β, ξ, and A as fitting parameters; the first two determine the shape of the function $I(p)$, while the latter only scales its overall magnitude. Our fits yield a coupling constant $\beta\sim0.09$ and $\xi\sim7$.[21] For comparison, we also plot the theoretical curves expected for $\beta=1,0.1,0.01$. In a conventional laser where $\beta\sim10^{-3}$, the photon number typically undergoes a sudden jump at threshold. Because of the high coupling constant of the cavity, the output power in these microdisk lasers increases with a finite slope around the transition region as shown in Fig. 2(a).

Figure 2(b) shows the power dependence of the energy and the full width at half maximum (FWHM) of the $TE_{35,1}$ laser mode. For pump power below 0.4 kW/cm^2, the peak energy undergoes a blueshift with increasing pump power because the refractive index decreases with increasing carrier density.[22] However, the plateau in the peak energy between 0.4 kW/cm^2 and 1.4 kW/cm^2 indicates that the blueshift is offset by local heating of the microdisk, eventually resulting in a redshift at the highest excitation densities. Below the threshold, we observe a spectral narrowing of the WGM as the excitation power increases. This indicates that the Q is limited by the absorption of the active layer at weak excitation.[1,3] Hence, it is more meaningful to estimate the Q of the microdisk at the transparency threshold which should lie just below the lasing threshold. At this excitation density, the FWHM is 0.288 meV while the emission wavelength is 1.61 eV, yielding an estimated $Q=E/\Delta E\sim5600$ for this mode. In comparison, similar estimates for the control samples with 4.2 nm and 10 nm QWs yield $Q\sim3000$ and 3500, respectively. Figure 2(b) shows that the FWHM undergoes an anomalous linewidth enhancement in the threshold region. The coupling between refractive index fluctuations and the carrier fluctuations in the gain medium may explain this broadening.[16] Above the threshold, the linewidth is inversely proportional to excitation power before the onset of heating, as indicated in the region between the two dashed lines in Fig. 2(b). This is described by a modification of the standard Schawlow-Townes formula, wherein the linewidth is multiplied by a factor $(1+\alpha^2)/2$, where α is the gain-refractive index coupling factor.

The temperature dependence of the emission spectra is measured in the range $6\text{ K}\leqslant T\leqslant70$ K with a fixed CW excitation of 1.8 kW/cm^2. Figure 2(c) shows that at high temperatures (between 50 K and 70 K), the laser emission cascades toward lower energies via three adjacent WGMs located between 1.61 eV and 1.59 eV (identified as $TE_{35,1}$, $TE_{30,2}$, and $TE_{26,3}$, respectively). Note that in spectra (1) and (2) of Fig. 2(c), the emission intensity of the $TE_{35,1}$ mode undergoes an abrupt transition toward the $TE_{30,2}$ mode, without exciting the higher order mode located in between. We attribute the observed mode switching to a combination of effects: the temperature dependence of the gain profile, narrowing of the band gap, and possibly the thermal excitation of electrons/holes from deeply confined 0D states to shallower QW states. We also observe mode hopping at low temperatures when the excitation power is large compared to the single-mode operation region discussed earlier [Fig. 2(d)]. Although the power-dependent mode hopping at low temperatures is also likely due to local heating of the microdisk (no changes are observed in the temperature sensor), we note that the transition from the $TE_{35,1}$ to the $TE_{30,2}$ mode is gradual, contrasting with the temperature-dependent changes shown in Fig. 2(c). We attribute this difference to the continued occupation of the 0D states at low temperatures as the pump power increases, as opposed to being depleted to higher states in fixed power/variable temperature measurements. Therefore, the $TE_{35,1}$ mode does not quench completely and the high carrier density can sustain multiple-mode operation.

Time-integrated measurements of the microdisk emission using pulsed excitation show spectral behavior that is similar to that obtained with CW excitation. In addition, we have measured the temporally and spectrally resolved emission spectra at different excitation powers [Fig. 3(a)]. Both the rise and decay of the emission become faster as the pump power exceeds the threshold (190 W/cm^2 for this particular microdisk). This is shown in Fig. 3(b), where the decay and delay time is plotted as a function of pump power. The decay time, defined as the $(1/e)$th time constant of the decay tail, is determined from exponential fits to the data. The delay (or rise) time is defined as the interval between the peaks of the

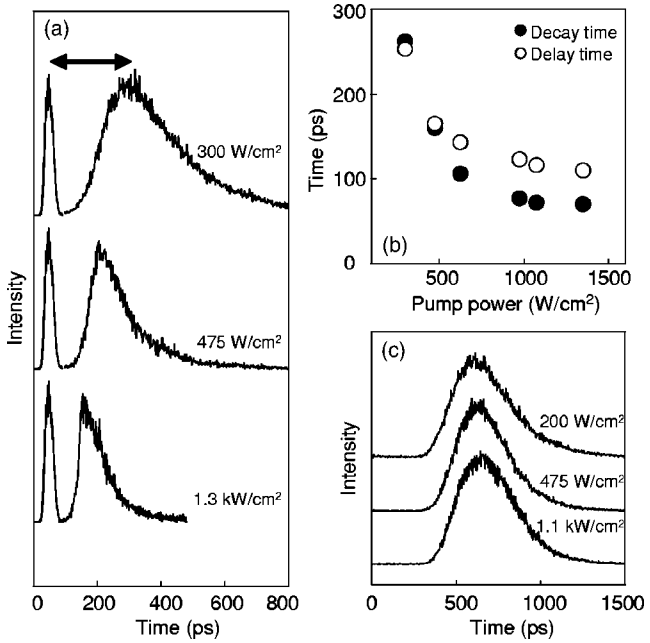

FIG. 3. (a) Temporal evolution of microdisk emission at 1.615 eV. Data at different pump intensities (indicated next to each spectrum) have been normalized and vertically shifted for clarity. The zero of time is fixed at the arrival of the excitation laser pulse (tuned to 1.676 eV). (b) Power dependence of decay and delay times. Decay time, defined as the $(1/e)$th time constant of the decay tail, is determined from exponential fits to the data. Delay time is defined as the interval between the peaks of the excitation and microdisk emission pulses [arrow in (a)]. Both show a marked decrease with increasing pump power. (c) The unprocessed part of the sample does not show any noticeable changes in either the pulse width or the delay time as input power is increased. All data in (a)–(c) are taken at 5 K.

excitation and microdisk emission pulses [arrow in Fig. 3(a)]. The fast rise and decay dynamics is due to the increased stimulated emission rate which is proportional to the photon number in the cavity mode and which dominates the emission spectra above the lasing threshold. A qualitatively similar temporal characteristic has been reported in earlier, spectrally integrated dynamical studies of GaAs/(Ga,Al)As microdisk QW lasers.[10] In contrast to the shortening cavity-photon lifetime as the pump power increases, the photon lifetime in the unprocessed IFQD sample is power-independent due to the lack of stimulated emission, as shown in Fig. 3(c).

Finally, we comment briefly on a comparison between the behavior of the microdisk sample with IFQDs and the control samples under pulsed excitation. The pump-power dependence of the decay times obtained for the control samples is almost identical to those observed for the IFQD sample, when the pump power is scaled by the threshold value (since the control samples have higher lasing threshold). However, we note that there are some differences: in the control samples, the peak intensity of the lasing mode is an order of magnitude smaller than that of the IFQD sample; the *spectrally integrated* time-resolved emission for the IFQD sample exhibits a single peak in the time domain, whereas the control sample with 10 nm QWs shows a second peak that appears for high pump power after a delay of $\sim 200-300$ ps. The latter behavior is similar to that reported in previous spectrally integrated studies of GaAs/(Ga,Al)As microdisk QW lasers where it was ascribed to carrier diffusion to the edges of the microdisk;[10] finally, the turn-on (delay) time for the 4.2 nm QW control sample is considerably longer than that of the IFQD sample. As supported by the spectrally integrated time-resolved data, carrier diffusion, which is the determining factor for the delay time, is limited in the IFQD sample compared to that seen in the control samples, which may be attributed to the presence of the IFQDs. This limitation of carrier diffusion may possibly be responsible for the better performance (larger Q and β, smaller threshold) of the microdisks with IFQDs.

In summary, we have investigated the static and dynamic response of a GaAs/(Ga,Al)As microdisk laser with IFQDs in the active region. Steady-state measurements of the stimulated emission yield a quality factor $Q \sim 5600$ and a coupling constant $\beta \sim 0.09$. The broad gain spectrum produces mode hopping between spectrally adjacent whispering gallery modes as a function of either temperature or excitation power. Time-resolved photoluminescence measurements show marked differences between the radiative decay rates in processed and unprocessed samples. The control samples without IFQDs display modes with smaller Q values and far lesser intensity. While, as mentioned earlier, the exact effect of the IFQDs is not easy to define, it seems amply clear that these microdisk lasers provide new templates for exploiting the interplay between 0D states and confined photons for quantum information processing.

This work was supported by the DARPA QuIST program, NSF-DMR, and Sun Microsystems. We thank E. Hu for critical comments, and R. Epstein, O. Maksimov, and M. Stone for technical advice at various stages of this project.

*Electronic address: nsamarth@psu.edu

[1] B. Gayral, J. M. Gérard, A. Lemaître, C. Dupuis, L. Manin, and J. L. Pelouard, Appl. Phys. Lett. **75**, 1908 (1999).

[2] A. Imamoglu, D. D. Awschalom, G. Burkard, D. P. DiVincenzo, D. Loss, M. Sherwin, and A. Small, Phys. Rev. Lett. **83**, 4204 (1999).

[3] P. Michler, A. Kiraz, Lidong Zhang, C. Becher, E. Hu, and A. Imamoglu, Appl. Phys. Lett. **77**, 184 (2000).

[4] H. Cao, J. Y. Xu, W. H. Xiang, Y. Ma, S.-H. Chang, S. T. Ho, and G. S. Solomon, Appl. Phys. Lett. **76**, 3519 (2000).

[5] P. Michler, A. Kiraz, C. Becher, W. V. Schoenfeld, P. M. Petroff, L. D. Zhang, E. Hu, and A. Imamoglu, Science **290**, 2282 (2000).

[6] D. K. Young, L. Zhang, D. D. Awschalom, and E. L. Hu, Phys.

Rev. B **66**, 081307(R) (2002).
[7] B. Gayral, J.-M. Gérard, B. Sermage, A. Lemaître, and C. Dupuis, Appl. Phys. Lett. **78**, 2828 (2001).
[8] L. Harris, D. J. Mowbray, M. S. Skolnick, M. Hopkinson, and G. Hill, Appl. Phys. Lett. **73**, 969 (1998).
[9] U. Mohideen, W. S. Hobson, S. J. Pearton, F. Ren, and R. E. Slusher, Appl. Phys. Lett. **64**, 1911 (1994).
[10] K. J. Luo, J. Y. Xu, H. Cao, Y. Ma, S. H. Chang, S. T. Ho, and G. S. Solomon, Appl. Phys. Lett. **77**, 2304 (2000).
[11] K. Brunner, G. Abstreiter, G. Bohm, G. Trankle, and G. Weimann, Phys. Rev. Lett. **73**, 1138 (1994).
[12] K. Brunner, G. Abstreiter, G. Bohm, G. Trankle, and G. Weimann, Appl. Phys. Lett. **64**, 3320 (1994).
[13] D. Gammon, E. S. Snow, and D. S. Katzer, Appl. Phys. Lett. **67**, 2391 (1995).
[14] J. Hours, S. Varoutsis, M. Gallart, J. Bloch, I. Robert-Philip, A. Cavanna, I. Abram, F. Laruelle, and J. M. Gerard, Appl. Phys. Lett. **82**, 2206 (2003).
[15] C. H. Henry, IEEE J. Quantum Electron. **QE-18**, 259 (1982).
[16] G. Bjork, A. Karlsson, and Y. Yamamoto, Appl. Phys. Lett. **60**, 304 (1992).
[17] M. K. Chin, D. Y. Chu, and S. T. Ho, J. Appl. Phys. **75**, 3302 (1994).
[18] R. E. Slusher, A. F. J. Levi, U. Mohideen, S. L. McCall, S. J. Pearton, and R. A. Logan, Appl. Phys. Lett. **63**, 1310 (1993).
[19] G. Bjork, A. Karlsson, and Y. Yamamoto, Phys. Rev. A **50**, 1675 (1994).
[20] G. Bjork and Y. Yamamoto, IEEE J. Quantum Electron. **27**, 2386 (1991).
[21] By definition, β and ξ are related by a proportionality factor. We have checked that the fit yields credible estimates for the physical parameters involved in this factor.
[22] U. Mohideen, R. E. Slusher, F. Jahnke, and S. W. Koch, Phys. Rev. Lett. **73**, 1785 (1994).